Sea ice concentration over the Antarctic Ocean from satellite pulse altimetry

YANG YuanDe[1]*, E DongChen[1], WANG HaiHong[2,3], CHAO DingBo[2],
HWANG CheinWay[4], LI Fei[1] & AI SongTao[1]

[1] *Chinese Antarctic Center of Surveying and Mapping, Wuhan University, Wuhan 430079, China;*
[2] *School of Geodesy and Geomatics, Wuhan University, Wuhan 430079, China;*
[3] *Key Laboratory of Surveying and Mapping Technology on Island and Reef, State Bureau of Surveying and Mapping, Qingdao 266510, China;*
[4] *Department of Civil Engineering, "National" Chiao Tung University, Hsinchu, Taiwan, China*

Sea ice concentration (SIC) is an important parameter in characterizing sea ice. Limited by the environment and the spatial extent of observation, it is difficult for field work to meet the needs of a large-scale SIC study. However, with its many advantages, such as the ability to make large-scale, high-resolution and long-duration observations, the altimeter can be used to determine SIC on a large scale. Using the correspondence between the satellite pulse altimeter waveform and reflector property, waveform classification is employed. Moreover, this paper develops an algorithm to obtain the SIC from altimeter waveforms. In an actual computation, Pyrz Bay in the Antarctic is taken as an experimental region, and one-year and seasonal SICs are derived from ERS-1/GM waveforms over this study area. Furthermore, altimetric SICs are compared with those of SSMR SSM/I. The results show that the spatial distribution and the regions of maximum SIC determined employing these two methods are consistent. This demonstrates that altimeter data can be used to monitor sea ice.

sea ice concentration, Antarctic, altimeter waveform, SSMR SSM/I, ERS-1/GM

Sea ice concentration (SIC) is the proportion of the ocean area actually covered by ice in an area. Because SIC reflects the dynamic change in ice sheets and shelves, and affects the interaction between the ocean and atmosphere, thus it has a crucial role in the ocean and atmosphere circulation. Therefore, information on the SIC is useful in the research on global climate change and shipping safety. However, it is difficult for a conventional research ship to pass through a region of sea ice. Moreover, because of technique difficulties, poor accuracy, high cost and a limited observation range, field work employing an icebreaker can not even meet the needs of a large-scale study on sea ice. Remote sensing, especially passive microwave sensing, is usually employed to obtain the SIC. For example, Cao and Jin [1] summarized the advantages and disadvantages of different remote sensing techniques. In addition, Wang et al. [2] used AMSR-E data to analyze the multi-year SICs of the Arctic Ocean.

One remote sensing technique uses a satellite microwave radar altimeter, which was initially designed for accurate measurements of marine gravity, sea surface height and geodynamics parameters [3]. Consequently, this technique records a large number of data to improve our understand-

*Corresponding author (email: yuande_yang@yahoo.com.cn)

ing of the ocean. Moreover, it has unique advantages, such as its ability to make all-day, all-weather, high-resolution, long-duration and global-scale observations. With the development of altimeter data processing, the applications of the satellite altimeter have been extended from ocean to non-ocean surfaces as well, such as the monitoring of inland water changes and determination of land topography in the investigation of crustal vertical motion [4–7]. However, there has been little application of satellite altimeter in studying the polar regions of sea ice.

A waveform is a direct measurement by a satellite radar altimeter. Because its shape is determined by the properties of the reflecting surface property, there is correspondence between the altimeter radar waveform and reflector. When two reflectors have a similar reflecting property, they generate similar waveforms, and vice versa. On the base of this relationship, many experiments have been carried out over different regions. For example, by analyzing waveforms reflected by polar regions, Laxon [8] demonstrated that sea ice mainly produces specular waveforms, which are very different from diffuse waveforms produced by open oceans.

Waveform classification can be employed to determine the waveform type corresponding to a certain reflector. Basic waveforms can be classified into categories of typical diffusion with only one leading edge over open-ocean, typical diffusion with multiple leading edges over coastal waters and diffuse-like pulses over sea ice. Some authors have carried out waveform retracking after obtaining the specular waveform from sea ice with the aim to improve the accuracy of the sea surface height and sea ice thickness [9–11]. This paper develops an index of the sea ice waveform to obtain the SIC and its spatial distribution over the Antarctic Ocean. Firstly, the waveform index is calculated for every altimeter waveform, with this index describing an average over the illuminated area. The index is then compared with a threshold value. A reflector with an index greater than the threshold value is identified as sea ice, and that with an index less than the value as ocean. Finally, the gridded SICs on a certain scale are precisely computed over the studied ocean.

1 Waveform data and SSMR SSM/I

Among different satellite altimeters, the coverage of the ERS series is almost global, up to 81.5°S–81.5°N, covering the entire Antarctic Ocean and part of the Arctic Ocean. Therefore, these data can be used to monitor sea ice over the Antarctic Ocean. ERS-1, launched in 1991, was the first European Remote Sensing Mission. Its objective is repeat measurements of the global environment. Typical observation cycles have periods of 3, 35 and 168 days, with the density of the 168-day geodetic mission (GM) phase being the highest among these phases. The altimeter data used in this paper are ERS.ALT.WAP obtained by AVISO in the

GM phase. These one-year data were collected from April 1994 to March 1995, and sampled at a rate of approximately 20 Hz. The cross-track spacing d_φ at latitude φ is a function of φ given by

$$d_\varphi = \cos\varphi \cdot d_0, \qquad (1)$$

where d_0 is the cross-track space at $\varphi \approx 0$, d_0 is about 8 km for ERS-1/GM data [12]. The experimental ocean Pyrz Bay has a latitude range of 55°–70°S. Hence, the mean resolution over this region is about 4 km.

To assess the effectiveness of the altimeter-derived SICs, SSMR SSM/I data, provided by the National Snow and Ice Data Center, are used as the remote sensing data in this paper [13]. These gridded data were obtained by Nimbus 7 SSMR and DMSP SSM/I sensors. Data were derived employing the NASA method, which is based on the polarization ratio and frequency gradient, and had 25 km×25 km spatial resolution, as well as daily and monthly temporal resolutions. Furthermore, the data are a polar stereographic projection, with a range of [0, 250]. Thus, the remotely sensed SCIs can be obtained from gridded data by multiplying by 0.4.

2 Altimeter waveform and waveform classification

An altimeter waveform is a curve of the return power versus time, sampled in setting time by an altimeter with automatic gain. According to the workings of the altimeter, the altimeter waveform consists of three parts: thermal noise, a rapidly rising leading edge and a decaying trailing edge. As the reflection of the ocean has a Gaussian distribution, the mean returned waveform over open-oceans can be expressed as [14]:

$$P(t) = \frac{A}{2}\left[erf\left(\frac{t}{\sqrt{2}\sigma} \right) + 1 \right]\begin{cases} 1, & t < 0, \\ \exp(-t/\alpha), & t \geqslant 0, \end{cases} \qquad (2)$$

where A is the amplitude of the waveform, σ controls the slope of the leading edge, t is the time difference between the sample time and the center of the leading edge, α is the exponential decay of the trailing edge, and erf is an error function. This type of waveform is referred to as an ocean waveform, and has a steep leading edge and a slowly decaying trailing edge.

The properties of the reflectance of sea ice differ from the assumptions of the Brown model, meaning that the sea ice waveform usually deviates from the ocean waveform. Figure 1 shows the typical waveforms for open ocean and sea ice. The ocean waveform with diffuse reflection is referred to as a diffuse waveform, while the typical sea ice waveform is referred to as a specular waveform, with specular or near-specular reflection. Both the leading and
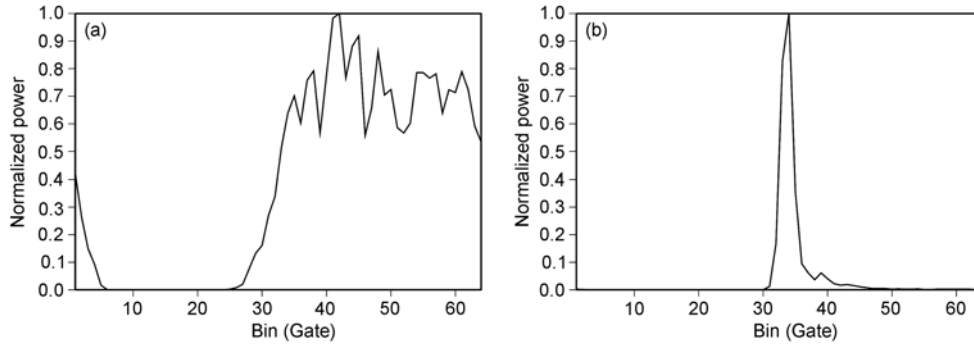
Figure 1 Typical waveform. (a) Open-ocean; (b) sea ice.

trailing edge of the specular waveform are steep, with the waveform being needle-like.

The key to monitoring sea ice via satellite altimeter is to detect a sea ice waveform or specular waveform. The aim of waveform classification is to identify the two waveform types. Dwyer and Godin [15] attempted to qualitatively analyze sea ice using waveforms obtained by satellite. Research on waveform classification began in 1994 when Laxon [8] found that the sea ice waveform differs from the open ocean waveform. Peacock and Laxon [9] developed the concept of pulse peakiness (*PP*) and successfully extracted the specular waveform over the Arctic Ocean. Pulse peakiness for the ERS-1 waveform is given by

$$PP = \frac{31.5 \times P_{\max}}{\sum_{i=5}^{64} P(i)}, \qquad (3)$$

where $P_{\max}$ is the waveform peak power and $P(i)$ is the power of the *i*th gate. The parameter *PP* is employed as the index of waveform classification in this paper. A threshold value of 1.8 is used to differentiate diffuse and specular waveforms. A waveform with *PP* less than 1.8 is determined to be diffuse and that with *PP* greater than 1.8 to be specular. Recently, *PP* has been widely used in waveform classification [6].

3 Sea ice concentration

The SIC, denoted *I*, on a grid can be obtained as

$$I = 100 \frac{S_I}{S}, \qquad (4)$$

where S_I and S are the area covered by ice and the entire area of the grid.

It is known that the altimeter waveform represents the mean over the illuminated area. In estimating the SIC, we make the following assumptions.

1) The altimeter waveform represents the mean SIC over the illuminated area, and the same radius *R* of the waveforms of the grid is considered.

2) The SIC *I* is equal to the average along-track SIC I_{track}.

Considering the resolution of SSMR SSM/I data, the SIC is calculated on a 12′×12′ grid. We suppose there are *N* tracks in a grid, with P_i waveforms corresponding to the *i*th track. The SIC of this grid is then estimated as follows.

1) We compute *PP* of the *j*th waveform corresponding to the *i*th track using eq. (3) and compare *PP* with 1.8 to identify the waveform type, with $W_{ij}=1$ for a specular waveform and $W_{ij}=0$ for a diffuse waveform.

2) We obtain the along-track sea ice area S_{Itrack} and the entire along-track area S_{track} for latitude φ_{ij} and waveform type W_{ij}:

$$\begin{aligned} S_{Itrack} &= \sum_{i=1}^{N} \sum_{j=1}^{P_i} \pi R^2 \cdot \cos\varphi_{ij} \cdot W_{ij}, \\ S_{track} &= \sum_{i=1}^{N} \sum_{j=1}^{P_i} \pi R^2 \cdot \cos\varphi_{ij}. \end{aligned} \qquad (5)$$

3) We substitute S_{Itrack} and S_{track} for S_I and S in eq. (4),

$$I_{track} = \sum_{i=1}^{N} \sum_{j=1}^{P_i} \pi R^2 \cdot \cos\varphi_{ij} \cdot W_{ij} \Big/ \sum_{i=1}^{N} \sum_{j=1}^{P_i} \pi R^2 \cdot \cos\varphi_{ij}.$$

According to the second assumption, $I=I_{track}$. When all waveforms across a grid are specular, then $S_{Itrack}=S_{track}$; i.e., $I=100$. However, when all waveforms are diffuse, $S_{Itrack}=0$ and $I=0$. The actual situation is between these the two cases, and hence, the range of *I* is 0–100.

4 One-year and seasonal SIC

Pyrz Bay is defined by 55°–95°E and 55°–72°S. Here, I_{ERS} and I_{SSM} represent the SICs obtained from the ERS-1/GM waveform data and SSMR SSM/I data. In this section, yearly and seasonal SICs and the distributions of I_{ERS} and I_{SSM} are estimated. These two results are compared and analyzed. Finally, the differences between the two methods are explained.

4.1 One-year SIC

The one-year I_{ERS} and I_{SSM} are obtained on a 12′×12′ grid

for Pyrz Bay, as shown in Figure 2. The figure shows that the two datasets for the one-year SICs have common features.

1) The datasets have similar sea ice distributions.

2) The datasets have overall agreement for regions of SIC maxima, such as regions around 64°, 74° and 83°E.

3) The datasets present a certain latitude zonation, where the SICs increase with increasing latitude.

However, there are clear differences between the two datasets shown in Figure 2.

1) I_{ERS} is greater than I_{SSM} overall.

2) The highest SICs are for high-latitude waters near land. However, the locations in Figure 2(a) are coastal waters near land, and the corresponding positions in Figure 2(b) are waters near land with a land boundary.

These two differences can be attributed to the following factors.

1) The satellite altimeter is more sensitive than SSMR SSM/I. Because the reflectivity of sea ice is greater than that of ocean, the waveform is specular even if there is less than 1% sea ice coverage in the illuminated area [9]. The grid is identified as sea ice if the *PP* is greater than the threshold value. However, Cao and Jin [1] showed that the pixel of a remote sensing image is very coarse for SSMR SSM/I. Therefore, when the waveform for a pixel with sea ice information is weak, the corresponding result may be corrupted. The NASA method was employed to obtain I_{SSM}; the result for spring is less accurate than that for autumn, and even less for summer as the ice melts. Furthermore, the results underestimate values over snowy and other primary sea ice and high-density sea ice. Hence, I_{ERS} is higher than I_{SSM}, such as in the case of maximum values.

2) The satellite radar waveform may be contaminated by reflectance from land as the altimeter approaches land. In this case, a complex waveform with multiple leading edges is received, and this waveform differs from a specular or diffuse waveform, making *PP* an invalid index of waveform classification. Therefore, I_{SSM} is more accurate than I_{ERS}

over water that is near land.

Table 1 shows the statistics of the one-year I_{ERS}, I_{SSM} and their difference $I_{ERS}-I_{SSM}$. To ensure the reliability of the results, $|I_{diff}|$ greater than 40 or $3\sigma_I$ is treated as an outlier. The distribution of I_{diff} is shown in Figure 2(c).

Table 1   Statistics of the one-year SICs

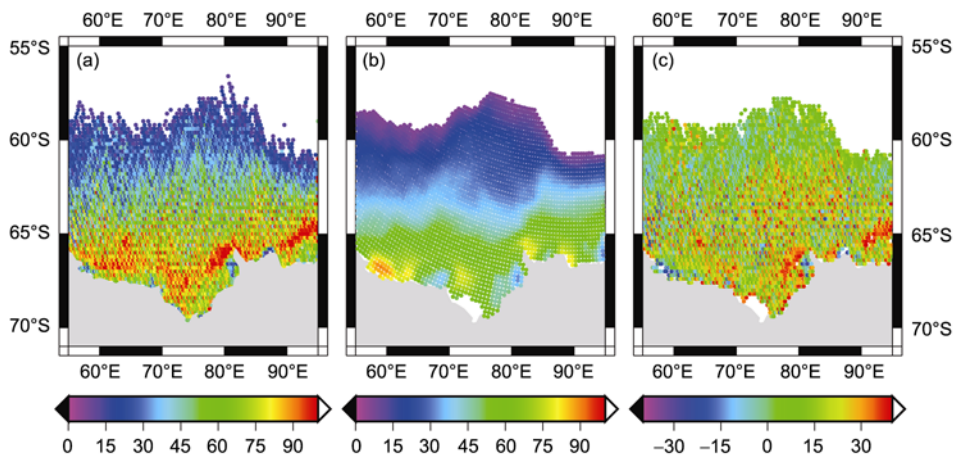| Data	Max	Min	Mean	Standard deviation
ERS-1/GM	100	10	54	±25
SSMR SSM/I	90	6	40.7	±19
I_{diff}	39.9	−27.8	12.5	±13.2

4.2   Seasonal change of sea ice concentration

In the Antarctic, spring is from August to October, summer from November to January, autumn from February to April and winter from May to June. The seasonal I_{ERS} values are calculated from 1994-04–1995-03 altimeter data, as shown in Figure 3(a), while the corresponding SSMR SSM/I result is shown in Figure 3(b).

Figure 3 shows that the seasonal SICs obtained employing the two different approaches have the following characteristics.

1) The SICs are the same for different seasons. For example, there is no sea ice around 68°, 80° and 93°E. However, the results show that altimetry can detect floating sea ice.

2) The derived SICs are similar.

3) Among the four seasons, the minimum sea ice distribution is in summer, with there even being regions without sea ice The extent of sea ice increases from autumn to spring, with the maximum being in spring.

Figure 3 shows that the seasonal I_{ERS} is greater than the overall I_{SSM}. Thus, the seasonal SICs are similar to the one-year result. The statistics are then derived for the four seasons (Table 2). The mean I_{diff} is about 14.8. The seasonal results differ, indicating different sea ice distributions, and

Figure 2   One-year SIC at Pyrz Bay. (a) I_{ERS}; (b) I_{SSM}; (c) $I_{ERS}-I_{SSM}$.
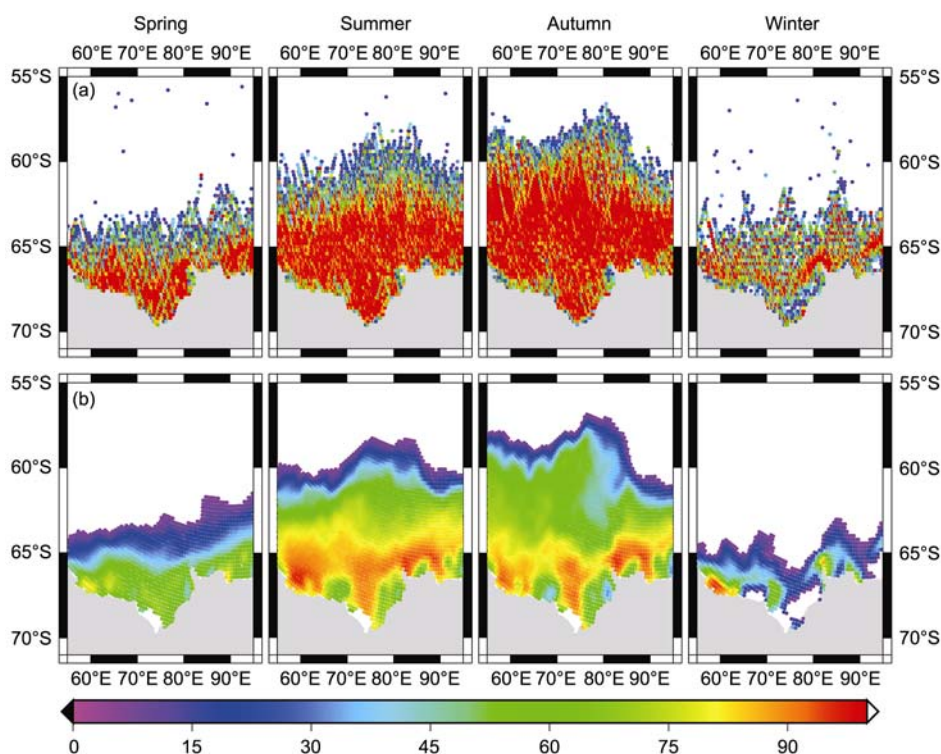
Figure 3 Seasonal changes in the SICs from 1994-04 to 1995-03 for Pyrz Bay. (a) ERS-1/GM; (b) SSMR SSM/I.

Table 2 Statistics of of differences in the seasonal SICs

Season	Max	Min	Mean	Standard deviation
Spring	39.9	−29.8	17.7	±14.7
Summer	39.9	−36.2	15.1	±16.9
Autumn	39.9	−37.7	16.3	±18.0
Winter	39.9	−36.0	10.3	±14.9

thus affect the result. For example, the summer sea ice distribution is less, which influences not only I_{SSM} in the NASA method but also the altimeter waveform and I_{ERS}. However, the statistics show that satellite altimetry is an effective tool to monitor sea ice.

5 Conclusions and discussions

Using the correspondence between an altimeter radar waveform and the reflector, this paper discussed the determination of the SICs and their distribution, and introduces the principle of determination and computation procedure. Pyrz Bay was taken as an experimental area, and the one-year SICs were obtained from ERS-1/GM waveforms. To assess the effectiveness of this method, the altimetric result was compared with SSMR SSM/I remote sensing data. The comparison showed that the two methods give similar spatial distributions of the sea ice and its concentration. However, it also indicated that the former result is overall

larger than the latter. The factors relating to the difference were analyzed, and difference statistics indicated that the method of determining the SIC via altimetry works well.

Moreover, seasonal SICs were derived from the same data. The results showed that the extent of the sea ice distribution is a minimum in summer, increases from autumn to spring and is at maximum in spring. Comparing the altimetry and remote sensing results also indicated that altimetry can be employed to monitor SICs. The results indicated that differences between the results of the two methods depend on the season.

To assess the method of determining the SIC effectively, the results of field work and altimetry need to be quantitatively compared. Factors affecting the difference, such as the sensitivity of the altimetric results to environmental change and the effects of assumptions, should then be mitigated. Finally, further research should involve complementary analysis of the altimetry and remote sensing results and determination of the SIC.

1   Cao M, Jin R. Sea ice Concentration monitor by Remote (in Chinese). Remote Sens Technol Appl, 2006, 21: 259–264

2   Wang H, Heygster G, Han S, et al. Arctic multiyear ice concentration retrieval based on AMSR-E 89 GHz data. Chin J Polar Res, 2009, 21: 186–196

3   Fu L L, Cazenave A. Satellite Altimetry and Earth Sciences. California: Academic Press, 2001

4   Jiang W, Chu Y, Li J, et al. Water level variation of Qinghai Lake from altimeteric data (in Chinese). Geomatics Inf Sci Wuhan Univ, 2008, 33: 15–18

5   Berry P A M, Jasper A, Bracke H. Retracking ERS-1 altimeter waveforms over land for topographic height determination: An expert system approach. ESA Pub, SP-414, 1997, 1: 403–408

6   Lee H K. Radar altimetry methods for solid earth geodynamics studies. Doctoral Dissertation. Columbus: Ohio State University, USA, 2008

7   Frédérique R, Soazig P. Antarctic ice sheet and radar altimetry: A Review. Remote Sens, 2009, 1: 1212–1239

8   Laxon S. Sea ice altimeter processing scheme at the EODC. Int J Remote Sens, 1994, 15: 915–924

9   Peacock N R, Laxon S. Sea surface height determination in the Arctic Ocean from ERS altimetry. J Geophys Res, 2004, 109: 1–14

10   Guo J, Gao Y, Hwang C, et al. A multi-subwaveform parametric retracker of the radar satellite altimetric waveform and recovery of gravity anomalies over coastal oceans. Sci China: Earth Sci, 2010, 53: 610–616

11   Hwang C, Guo J, Deng X, et al. Coastal gravity anomalies from retreacked Geosat/GM altimetry: Improvement, limitation and the role of airborne gravity data. J Geodesy, 2006, 80: 204–216

12   Sandwell D T, Smith W H F. Marine gravity anomaly from Geosat and ERS-1 satellite altimeter. Geophys J Int, 2005, 163: 79–89

13   Cavalieri D, Parkinson C, Gloersen P, et al. Sea ice concentrations from Nimbus-7 SMMR and DMSP SSM/I passive microwave data. Boulder, Colorado USA: National Snow and Ice Data Center, 1996, updated 2008

14   Brown G S. The average impulse response of a rough surface and its applications. IEEE Trans Anttennas Propag, 1977, AP-25: 67–74

15   Dwyer R E, Godin R H. Determining sea-ice boundaries and ice roughness using GEOS-3 altimeter data. NASA Contractor Report, NASA, 1980